ChemPubSoc Europe

DOI: 10.1002/open.201800277

Open Access ChemistryOPEN Full Papers

Mix-&-Read Determination of Mercury(II) at Trace Levels with Hybrid Mesoporous Silica Materials Incorporating Fluorescent Probes by a Simple Mix-&-Load Technique

Estela Climent,[a] Mandy Hecht,[a, b] Heike Witthuhn,[a] Kornelia Gawlitza,[a] and Knut Rurack*[a]

Dedicated to Dr. Norbert Jakubowski on the occasion of his 65th birthday

The synthesis, characterization, and application of mesoporous materials containing boron–dipyrromethene (BODIPY) moieties that allow the sensitive and selective detection of Hg^{II} in aqueous environments by fluorescence enhancement is reported. For this purpose, BODIPY dye **I** containing a thia-aza crown ether receptor as the fluorescent probe for the detection of Hg^{II} in aqueous environments is encapsulated into mesoporous materials to avoid self-quenching or aggregation in water. Determination of Hg^{II} is accomplished within a few seconds with high selectivity and sensitivity, reaching a limit of detection of 12 ppt. The determination of trace amounts of Hg^{II} in natural waters and in fish extracts is demonstrated by using our sensing material. The incorporation of the material into several μ-PAD strips yields a portable, cheap, quick, and easy-to-handle tool for trace Hg^{II} analysis in water.

1. Introduction

Mercury is a bioaccumulating and highly toxic heavy metal that causes serious human health problems even at low concentrations, most of all through contamination of drinking water and other natural water resources.[1–4] This dangerous metal is accumulated in living organisms mainly in its methylated form (CH_3Hg^+), most prominently in fish tissue along the food chain.[5–7] In fish tissue, mercury concentrations are frequently higher than the maximum levels recommended. The European Commission Decision 1881/2006 sets the maximum limit for mercury in seafood at 500 $\mu g\,kg^{-1}$ for fresh food, increasing to 1000 $\mu g\,kg^{-1}$ for the edible parts of some listed species that, for physiological reasons, concentrate mercury more easily in their tissues.[8] The maximum contaminant level for drinking water is thus also set at very low values, for example, 2 ppb according to the U. S. Environmental Protection Agency.[3] Owing to the growing awareness of the population for food and water safety and to facilitate the work of food inspectors or other authorities responsible for controlling food and water or to uncover environmental misconduct, simple and cheap tests for the selective trace detection of contaminants such as Hg^{II} are required. Because Hg^{II} has been an environmental problem for more than a century, a number of methods for its detection by considerably simple means have been published, for example, based on sensors operating electrochemically[9,10] or spectroscopically, the latter including colorimetric,[11] fluorometric, and Raman spectroscopic approaches.[12–16] With respect to probes and indicators employed, functionalized nanomaterials such as plasmonically active metal nanoparticles,[17–19] semiconductor nanocrystals, carbon nanotubes,[20,21] and graphene have caught up with the traditionally used indicator molecules.[22–24] Frequently, nanoparticles have especially been combined with biomolecules such as enzymes[25] and oligonucleotides.[26–31] Regarding simplicity and use in random inspections or suspicious cases, disposable strip-based tests are perhaps the most appealing format,[32] whereas the usually more elaborate and expensive microfluidic devices are much better suited for in-line monitoring purposes.[16,33,34] Strip tests do not require specific skills, are usually cheap and robust, and provide the analytical result within a reasonably short time.[14,35–37] Unfortunately, many of these tests have limitations with respect to sensitivity and quantification.

Herein, we report the synthesis, characterization, and application of organically functionalized mesoporous silica materials containing boron–dipyrromethene (BODIPY) indicators that allow for the sensitive and selective determination of Hg^{II} in aqueous environments by fluorescence enhancement. For this purpose, BODIPY probe **I** possessing a thia-aza crown ether re-

[a] Dr. E. Climent, Dr. M. Hecht, H. Witthuhn, Dr. K. Gawlitza, Dr. K. Rurack
Department of Analytical Chemistry; Reference Materials
Bundesanstalt für Materialforschung und -prüfung (BAM)
Richard-Willstätter-Str. 11 12489 Berlin (Germany)
E-mail: knut.rurack@bam.de

[b] Dr. M. Hecht
Current address:
CodeCheck GmbH
Gneisenaustraße 115, 10961 Berlin (Germany)

Supporting Information and the ORCID identification number(s) for the author(s) of this article can be found under: https://doi.org/10.1002/open.201800277.

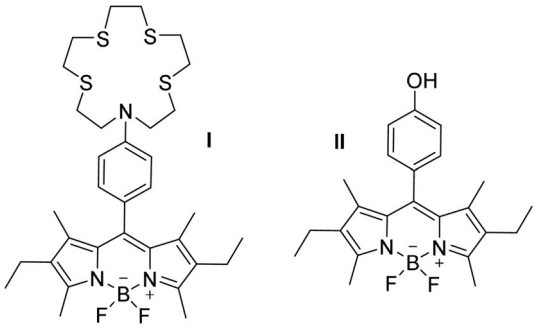

Scheme 1. Chemical structures of BODIPY dyes **I** and **II**.

ceptor that is ideal for Hg^{II} complexation[38–40] was synthesized (Scheme 1) in analogy to a probe reported earlier by us.[41] BODIPY dyes are notable for their high molar absorption coefficients, high fluorescence quantum yields, small Stokes shift, and good photo- and chemical stability,[41–43] but self-quenching and aggregation in water are major problems for such dyes that are to be used as molecular probes directly in realistic samples.[44,45] Commonly, these aggregates stem from π–π stacking, and they are, like BODIPY dimers, only very weakly or entirely nonemissive.[42,46] It is, therefore, necessary to prevent aggregation, which is commonly accomplished by introducing solubilizing substituents such as poly(ethylene glycol) (PEG) chains,[47,48] sulfonic acid groups,[49,50] or betaine groups.[51] As all of these approaches require partly rather sophisticated synthetic pathways, especially if BODIPYs are multiply functionalized to be used as probes or indicators, we strived to embed the probes only sterically into mesoporous silicas. Our strategy was based on the following considerations. With respect to polarity, the inner pore walls of mesoporous silica are rather hydrophobic,[52] comparable to solvents such as ethyl acetate.[53] We, thus, rationalized that the choice of sufficiently hydrophobic probes should make it possible to load the probes into the pores simply by mixing the porous nanomaterial and a dye solution, as the strong adsorption forces of the mesopores' inner surface would prevent the dyes from leaching.[54] Moreover, with respect to system optimization, the polarity of the inner (and outer, separately or in combination) surfaces can be tuned in a facile manner by silanization with organic groups.[53] As BODIPYs possess high *n*-octanol/water partition coefficient (K_{OW}) values,[55] not only did we expect the probes to reside in adequately tailored pores, but we also expected aggregation to be largely avoided. If applied for metal-ion detection in aqueous solution, entry of such ionic species into the water-filled pores should be easily possible, and because of the small dimensions and the considerably low polarity at the interface between pore wall and pore void,[56] binding at the probe's receptor should become feasible, especially if binding constants are high, as the reduced polarity would eventually even enhance recognition.[57] On the basis of our earlier studies,[46,53,56] we thus prepared a variety of silica materials modified with different organic groups to create several specific environments and to screen for the best hybrid support. In addition, we encapsulated **I** in MCM-41 and SBA-15 to evaluate the effect of pore size on potential aggregation inside the mesochannels. Among all the materials tested, xPRO-SBA-**I**, consisting of a mesoporous SBA-15 silica functionalized selectively with propyl groups on the outer surface, performed best, and it allowed for a limit of detection for Hg^{II} determination of 12 ppt in water at neutral pH.

2. Results and Discussion

2.1. Spectroscopic Properties of I

The spectroscopic properties of **I** in acetonitrile (MeCN) and in water are presented in Figure 1. As can be seen, the spectroscopic features are somewhat different. In MeCN, **I** shows a narrow absorption band typical for symmetrically hexaalkyl-substituted BODIPY dyes with a maximum at $\lambda = 520$ nm ($\varepsilon = 69\,300\ M^{-1}\,cm^{-1}$),[58] represented by a pink color of the solution. In aqueous environments at low concentration, a moderate tendency for dimer/aggregate formation is visible by a certain broadening of the absorption band ($\lambda = 532$ nm, $\varepsilon = 40\,500\ M^{-1}\,cm^{-1}$) and the correspondingly higher mismatch of the fluorescence excitation and absorption spectra.[45] Fluorescence emission of the BODIPY probe is low in both solvents, showing global emission maxima at $\lambda = 535$ and 550 nm ($\lambda_{ex} = 490$ nm) with fluorescence quantum yields (Φ_f) of < 0.001 and < 0.002 in MeCN and water, respectively. Furthermore, a second, redshifted emission band, at $\lambda = 735$ nm in MeCN and $\lambda = 675$ nm in water, is observed that is characteristic of spectrally broad fluorescence arising from intramolecular charge-transfer (ICT) states of *meso*-anilino-substituted BODIPYs.[41,59] Thus, at 1 μM, the step from the polar, nonprotic organic solvent to the aqueous medium reflects the change in the solvent's dielectric constant and hydrogen-bonding properties, with aggregation or dimerization playing a certain role in the aqueous environment.[45]

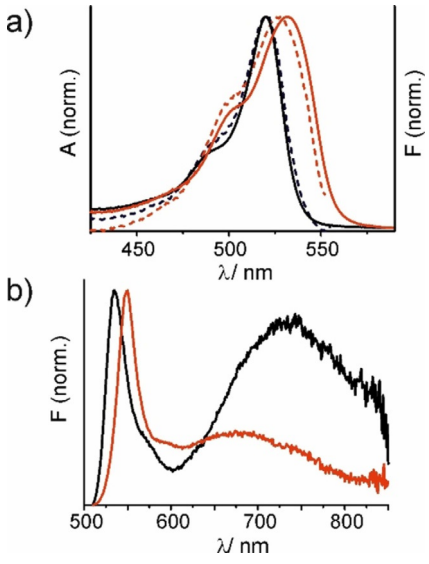

Figure 1. a) Absorption spectra (solid lines) and fluorescence excitation spectra ($\lambda_{em} = 564$ nm; dashed lines) of BODIPY dye **I** ($c = 1.6$ μM) in MeCN (black) and in Milli-Q water at pH 7 (red). b) Corresponding fluorescence emission spectra ($\lambda_{ex} = 490$ nm) of **I** in MeCN (black) and Milli-Q water at pH 7 (red).

2.2. Analytical Response of I

meso-Receptor-substituted BODIPY dyes are principally very potent probes, because they allow for strong switching of the fluorescence upon analyte binding.[41,60,61] The complexation behavior of **I** was thus investigated in more detail in the presence of the thiophilic metal ions Hg^{II} and Ag^{I} and their closest paramagnetic competitors, Cu^{II} and Ni^{II}. These cations were added at a final concentration of 1 ppm to solutions of **I** (c_I = 1.1 μM) in MeCN and H_2O, and the absorption and emission spectra were recorded (Figure 2). It is clear that the reaction between **I** and the four metal ions proceeds differently in MeCN than in water. The absorption spectra in MeCN offer minor changes upon complex formation, and a strong fluorescence enhancement is observed only with Ag^{I} and Hg^{II} (Figure 2c,d). In water, the absorption spectra reveal complex formation only for Hg^{II}, as exemplified by hypo- and hyperchromic effects. The narrowing of the band upon Hg^{II} binding further suggests that aggregates or dimers are broken up once the cation is bound. Furthermore, whereas Cu^{II} and Ni^{II} are not able to produce any fluorescence enhancement and the effect of Ag^{I} is rather weak, Hg^{II} is still able to generate a favorably large enhancement factor EF_{Hg} = 175 (vs. EF_{Ag} = 3.5 for Ag^{I}; i.e., a discrimination factor $DF_{Hg/Ag} = EF_{Hg}/EF_{Ag}$ = 50; Figure 2b). This excellent discrimination of mercury against the other cations is not observed in MeCN ($DF_{Hg/Ag}$ = 1.2) and is ascribed to the relative gain in solvation of the metal ions in water at the expense of the complex stability constant; this influence is more pronounced for Ag^{I} because of the distinctly lower complex stability[41,62] of this monovalent ion. Furthermore, the higher affinity of the receptor for Hg^{II} is also expected to facilitate dissociation of any dimers or aggregates.

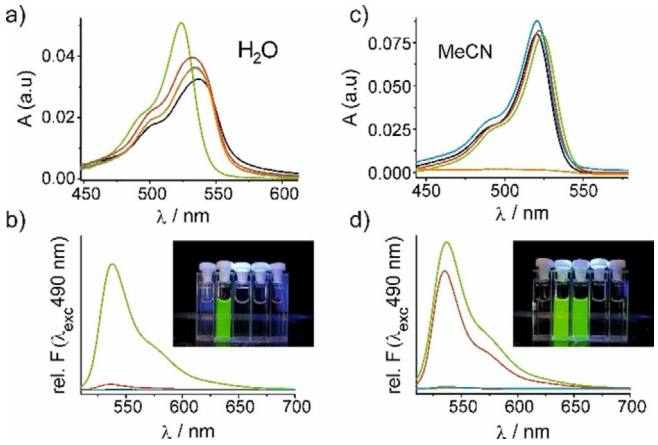

Figure 2. Absorption spectra of BODIPY dye **I** (1.1 μM; black lines) in a) water and c) MeCN in the absence and in the presence of 1 ppm of cations Hg^{II} (green line), Ag^{I} (red line), Ni^{II} (blue line), and Cu^{II} (orange line; the bleaching behavior of Cu^{II}, which only occurs in MeCN yet not in H_2O or aq. MeCN, was observed before, see Ref. [41]). Corresponding fluorescence emission spectra (λ_{ex} = 490 nm) of **I** (1.1 μM) in b) Milli-Q water at pH 7 and d) MeCN. Inset bottom: Corresponding photographs under UV light (λ_{ex} = 365 nm) of an initial solution of BODIPY **I** dye (1.1 μM) in the presence of (from left to right) 1 ppm of Hg^{II}, Ag^{I}, Ni^{II}, and Cu^{II}.

Aiming at real-time Hg^{II} indication, we next studied the binding kinetics and analyzed the change in fluorescence at λ = 540 nm of a solution of **I** (1.7 μM in H_2O at pH 7) as a function of time in the presence of 500 ppb of Hg^{II} (Figure 3a). Whereas no change in fluorescence was observed in the absence of Hg^{II}, a fast signal increase was observed in the presence of the heavy-metal ion. Fitting the data to a pseudo-first-order kinetic reaction model under the assumption that the fluorescence increase depended only on the concentration of Hg^{II}, a rate constant of 0.024 s^{-1} and a half-life ($t_{1/2} = \ln 2/k$) of $t_{1/2}$ = 28.8 s were determined. Next, we evaluated the sensitivity of the response of **I**. The absorption and fluorescence excitation and emission spectra of **I** (1.1 μM) were recorded in Milli-Q water upon titration with Hg^{II} (Figures 3b–d). Due to the fast response, kinetics spectra were taken roughly 45 s after the addition of Hg^{II}. The UV/Vis titrations revealed that upon the addition of more than 0.35 ppm of Hg^{II}, the absorption band became narrowed and blueshifted from λ = 532 to 524 nm, accompanied by an increase in extinction. At concentrations >0.8 ppm, the color of the solution changed from pink to yellow, which was visible to the naked eye (Figures 3b, inset; also see Figure S1 in the Supporting Information).

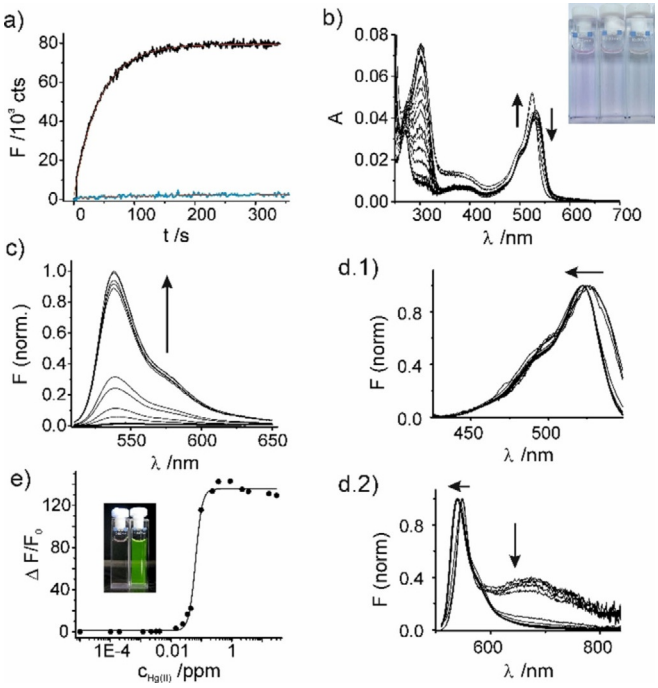

Figure 3. a) Fluorescence intensity at λ = 540 nm of **I** in water (1.7 μM in H_2O at pH 7; λ_{ex} = 490 nm) registered as a function of time while stirring the solution in a cuvette in the absence (blue line) and presence (black line) of Hg^{II} (500 ppb). Red lines correspond to fits of the data to a first-order kinetic reaction model. b) Absorption spectra of **I** (1.7 μM, Milli-Q water, pH 7) in the absence and in the presence of Hg^{II} (0–3 ppm). Inset: Photograph showing the color changing from pink to yellow; see also Figure S1 for a larger version. From left to right, c_{Hg} = 0, 0.1, and 0.8 ppm. c) Corresponding fluorescence spectra (λ_{ex} = 490 nm). d) Normalized excitation (d.1, top; λ_{em} = 564 nm) and emission (d.2, bottom; λ_{ex} = 490 nm) titration spectra. e) Plot of fluorescence enhancement ratio, $\Delta F/F_0$, that is, $(F-F_0)/F_0$, registered at λ = 538 nm (λ_{ex} = 490 nm) as a function of Hg^{II} added. Inset: Photograph showing change in fluorescence under UV light (λ_{ex} = 365 nm) in the absence and in the presence of Hg^{II} (2 ppm).

From the titrations, we could also deduce that the addition of higher amounts of Hg^{II} broke up dye aggregates or dimers in aqueous solution. Furthermore, the fluorescence spectra again revealed a strong increase in the typical BODIPY fluorescence (Figure 3c), reaching a final $\Phi_f = 0.63$ for the **I**–Hg^{II} complex. As would be expected for ICT probes, complexation of the metal ion at the electron-donating receptor moiety concomitantly quenched the redshifted ICT fluorescence (Figure 3d, bottom). Due to a change in the inductive effect of the *meso* substituent upon Hg^{II} binding, the BODIPY-type emission maximum was displaced to the blue by about $\Delta\lambda = 10$ nm. Analysis of the fluorescence titration data by a four-parameter logistic function yielded an acceptable fit, determining the limit of detection (LOD, 3σ-method) to 3 ppb for **I** at around 2 μM and Hg^{II} in aqueous solution. Our method is thus much more sensitive than other approaches relying on BODIPY derivatives[63,64] and achieves an outstanding discrimination against Ag^{I}, Ni^{II}, and Cu^{II} in water.[65] Fluorescence lifetime measurements of **I** and **I**–Hg^{II} in MeCN and water supported the steady-state findings. In accordance with more than one emitting species and a potential ground-state species diversity of crown ethers, especially in water,[59] the decays of **I** were fitted to a multiexponential decay (see Section S7). Indeed, as shown in Table 1, a biexponential decay was sufficient to fit the data in both solvents in the absence of Hg^{II} with acceptable goodness. In the presence of Hg^{II}, not only did the fluorescence decay time increase dramatically but the kinetics became monoexponential, in agreement with a single complex species showing chelation-enhanced fluorescence.[66]

Table 1. Fluorescence lifetimes of **I** in H_2O and MeCN in the absence and presence of Hg^{II}.[a]

Species	Solvent	τ_1 [ns]	τ_2 [ns]	α_1 [%]	α_2 [%]
I	H_2O	0.025	1.81	0.97	0.03
I–Hg^{II}	H_2O	–	5.63	–	100
I	MeCN	0.03	2.25	0.99	0.01
I–Hg^{II}	MeCN	–	5.26	–	100

[a] $\lambda_{ex} = 488$ nm, $\lambda_{em} = 540$ nm, see Figure S9 for decays. α = relative amplitude.

2.3. Incorporation of I into Mesoporous Silicas

Despite complexation of **I** with Hg^{II} offering a fast response and excellent selectivity, the LOD was not sufficient for unequivocal Hg^{II} determination in the required concentration range, presumably also connected to the dimerization/aggregation tendency of **I** in water. Moreover, due to the susceptibility of the ICT process active in **I** on environmental modulations, it was deemed crucial to us to improve the performance of the probe by incorporating it into a porous host material. To keep the design simple, integration was targeted only by the mix-&-load technique, that is, by suspending the material in a solution containing the probe, followed by stirring for a certain time, centrifuging, washing, drying, and then having the sensor material already at hand for its application. Key to finding the optimal material for hosting **I** was, thus, to screen various pore sizes and surface functionalizations. We, therefore, prepared several mesoporous silica nanomaterials of the MCM-41 and SBA-15 types modified with amino, poly(ethylene glycol), epoxy, and propyl groups to create environments of different polarities and proticities at the surface and/or inside the pores. Here, SBA-15 particles of about 1 μm diameter possess a specific surface area of roughly 800 $m^2 g^{-1}$ and a pore diameter of around 8 nm. For the MCM-41 particles, with a specific surface area close to 1000 $m^2 g^{-1}$ and a pore diameter of about 2.5 nm, nanoparticles of approximately 100 nm diameter were chosen to avoid problems due to long diffusion paths in the narrow channels. In addition, bulk silica nanoparticles (N) of around 450 nm diameter and with a specific surface area of 50 $m^2 g^{-1}$ were used as nonporous controls. The library prepared consisted of 17 materials that were all sterically loaded with **I** by simply stirring a suspension at room temperature for 24 h: unmodified, extracted SBA-15, MCM-41, and bulk silica particles (SBA-**I**, MCM-**I**, N-**I**); extracted mesoporous materials and bulk particles uniformly modified on the inner and outer surfaces with aminopropyltrimethoxysilane (APT-SBA-**I**, APT-MCM-**I**, APT-N-**I**), 2-{methoxy[poly(ethylene oxy)]propyl}trimethoxysilane (PEG-SBA-**I**, PEG-MCM-**I**, PEG-N-**I**), 3-glycidoxypropyltrimethoxysilane (EPO-SBA-**I**, EPO-MCM-**I**, EPO-N-**I**), and propyltrimethoxysilane (PRO-SBA-**I**, PRO-MCM-**I**, PRO-N-**I**); and extracted mesoporous materials modified only on the external surface with propyltrimethoxysilane (xPRO-SBA-**I**, xPRO-MCM-**I**). To optimize the system with respect to the amount of **I** loaded into the materials, a more concentrated solution of **I** (1.05 mmol L^{-1} vs. 26 μmol L^{-1}) was used for the mix-&-load preparation of the three best-performing materials, arriving at SBA-**I**′, APT-SBA-**I**′, and xPRO-SBA-**I**′. For comparison, and because the N-type materials loaded with a lower amount of **I** showed essentially no response, we also prepared materials N-**I**′, APT-N-**I**′, PEG-N-**I**′, EPO-N-**I**′, and PRO-N-**I**′. Scheme S1 collects an overview, and Section S1 provides all of the synthetic details of the library of materials. For the best-performing sensor material, a control material was also prepared with dye **II** (Scheme 1) that does not respond to Hg^{II}, namely, xPRO-SBA-**II**.

2.3.1. Spectroscopic Properties of xPRO-SBA-I

After prescreening all of the materials prepared with regard to their response against Hg^{II}, xPRO-SBA-**I**, consisting of mesoporous SBA-15 silica particles functionalized selectively with propyl groups on the outer surface and containing a considerably low amount of **I** adsorbed at the inner pore walls, was singled out as the best-performing material and was investigated spectroscopically in more detail. Figure 4a shows the absorption and fluorescence excitation and emission spectra of a suspension of xPRO-SBA-**I** in water. Both the excitation and absorption spectra look virtually identical, and this is indicative of the absence of dimers or aggregates. Furthermore, the maxima in the absorption and emission spectra are centered at $\lambda = 520$ and 538 nm, respectively; these values closely resemble the maxima of **II** at neutral pH in ethanol/water = 1:1, that is, media in which no dimers or aggregates are present.[45]

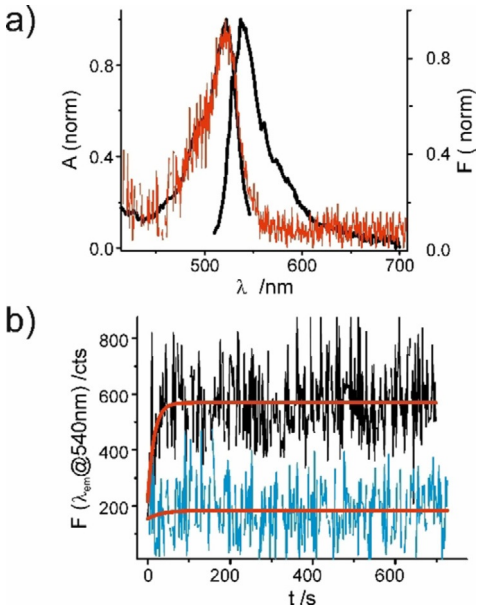

Figure 4. a) Absorption (solid red line) and fluorescence excitation ($\lambda_{em}=564$ nm) and emission spectra ($\lambda_{ex}=490$ nm; solid black lines) of xPRO-SBA-**I** in Milli-Q water (0.11 mg mL^{-1}, pH 7). b) Fluorescence intensity registered at $\lambda=538$ nm ($\lambda_{ex}=490$ nm) of xPRO-SBA-**I** in Milli-Q water (0.11 mg mL^{-1}, pH 7) as a function of time in the absence (blue line) and presence (black line) of Hg^{II} (500 ppb). Note that a suspension of blank xPRO-SBA (containing no dye) at the respective concentration was used to correct for scattered light in the absorption spectrum.

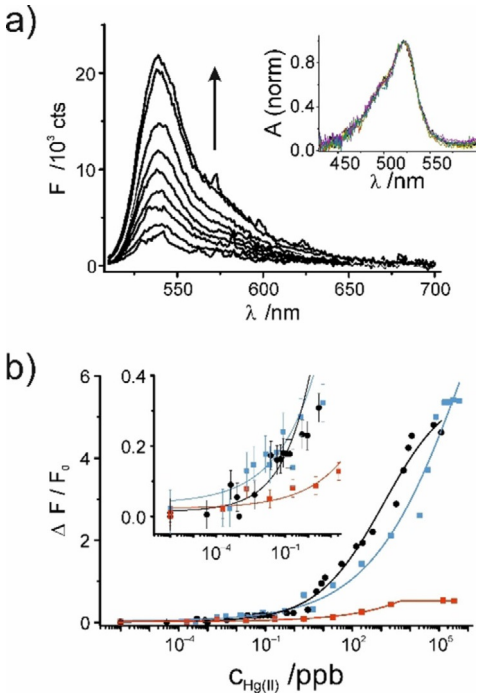

Figure 5. a) Fluorescence emission spectra ($\lambda_{ex}=490$ nm) of xPRO-SBA-**I** (0.11 mg mL^{-1} in Milli-Q water, pH 7) in the presence of different amounts of Hg^{II}. Inset: Corresponding normalized absorption spectra. b) Corresponding fluorescence enhancement ratio ($\Delta F/F_0$) registered at $\lambda=538$ nm ($\lambda_{ex}=490$ nm) as a function of Hg^{II} added in Milli-Q Water (black line, pH 7), acetate buffer (red line; 10 mM, pH 4), and phosphate buffer (blue line; 10 mM. pH 7). Inset: Magnification of the low-concentration range.

Apparently, the assembly of the material by the simple mix-&-load technique leads to a hybrid in which BODIPY probes are adsorbed in a monomeric form at the inner walls of the pores, avoiding any unwanted aggregation.

2.3.2. Response to Hg^{II}

Having established the spectroscopically favorable nature of **I** in xPRO-SBA-**I**, we were interested in assessing the binding kinetics of the material, a key criterion for rapid tests. Like before, the kinetic run was performed in the absence and presence of 500 ppb of Hg^{II}. Figure 4b again reveals a fast rise in the fluorescence signal only in the presence of Hg^{II}, similar to that observed for neat **I** in aqueous solution (Figure 3a). The rate constant and half-life were determined to be $k=0.067$ s^{-1} and $t_{1/2}=10.3$ s, respectively, indicating that diffusion of the metal ions into the porous materials is virtually unhindered. The fact that the response time of the hybrid system is even faster than that of neat **I** in solution can tentatively be ascribed to aggregation of the latter. In neat aqueous solution, Hg^{II} has to break up the nonfluorescent aggregates[67] of **I** first, before fluorescence of **I**–Hg^{II} can be recorded. In contrast, **I** is much less aggregated in xPRO-SBA-**I**, and this allows for faster binding with an instantaneous fluorescence increase.

The sensitivity of xPRO-SBA-**I** was evaluated in Milli-Q water and at different pH values by employing acetate buffer (10 mM, pH 4) and phosphate buffer (10 mM, pH 7), see Figure 5. In all cases, the emission band was centered at $\lambda=$ 538 nm, and the fluorescence enhancement correlated with the Hg^{II} concentration during a titration. The fact that Hg^{II} did not produce any sizable displacement of the absorption or emission maximum (Figure 5a) is more proof for the absence of any aggregation of the sterically incorporated dye molecules. The limits of detection (LODs) were again derived, as mentioned above, arriving at values of 12, 19, and 32 ppt in Milli-Q water, phosphate buffer, and acetate buffer, respectively. Moreover, Figure 5b indicates that the enhancement in fluorescence was significantly lower at acidic pH values. The latter can be ascribed to a more acidic environment if residual silanol groups at the surface of xPRO-SBA-**I** are partially protonated at pH 4, as they are thus able to interact with **I**, which leads to enhanced fluorescence in the absence of Hg^{II}. Accordingly, the fluorescence of xPRO-SBA-**I** is about three times higher at pH 4 than at pH 7. Nonetheless, the sensitivities found between pH 4 and 10 were very similar. From these experiments, we can conclude that adsorption of **I** inside a properly modified mesoporous SBA material increases the sensitivity dramatically from roughly 3 ppb (free **I** in H_2O solution) to about 15 ppt, presumably due to the inhibition of dimerization/aggregation of the probe and facilitation of complex formation at the interface of reduced polarity inside the pores. Furthermore, these LODs are in all cases well below the maximum permissible concentrations of Hg^{II} in drinking water.[3] Hence, xPRO-SBA-**I** should be an ideal candidate as a sensitive and selective rapid test for Hg^{II} trace determination in aqueous samples.

2.3.3. Role of BODIPY Dimers/Aggregates

From the point of view of system design, it is important to corroborate our tentative explanation that the absence of aggregation is responsible for the 150-fold gain in sensitivity. Therefore, we prepared and investigated xPRO-SBA-**I**′, a twin of xPRO-SBA-**I** that is loaded with 40 times more dye. Whereas the fluorescence excitation and emission spectra of aqueous suspensions of xPRO-SBA-**I**′ showed bands that were identical to those of xPRO-SBA-**I**, the absorption band was significantly broadened with respect to the fluorescence excitation spectrum, indicating the presence of nonfluorescent aggregates (Figure 6a).[45,46] Accordingly, the initial fluorescence of the material was also higher than that of xPRO-SBA-**I**, yet not 40 times but only 10 times. Titrations with Hg^{II} were then performed by following the same procedure as that described before by using suspensions of xPRO-SBA-**I**′ at 0.11 mg mL^{-1}. The UV/Vis titration curve shows a slight redshift and narrowing of the band (Figure 6b), accompanied by a higher fluorescence enhancement than that recorded for xPRO-SBA-**I** (Figure 6c vs. Figure 5a). Despite this higher enhancement, the hybrid showed a worse LOD of 0.96 ppb, which is around 80 times lower than the LOD of xPRO-SBA-**I**. This worse performance can, thus, be ascribed to the presence of dimers/aggregates in the pores of xPRO-SBA-**I**′ that hamper complexation despite the fact that Hg^{II} could produce an overall higher enhancement because of deaggregation.

Analysis of the fluorescence decay profiles of suspensions of xPRO-SBA-**I** and xPRO-SBA-**I**′ in water in the presence of different concentrations of Hg^{II} supported our findings. Nonexponential decay kinetics with bi- or multimodal distributions were found in the absence and presence of Hg^{II}. Whereas in the absence of Hg^{II} the average fluorescence lifetimes were determined to 1.8 and 1.3 ns for xPRO-SBA-**I** and xPRO-SBA-**I**′, respectively, the presence of Hg^{II} led to a significant increase in τ_{av} as a function of the concentration, resulting in values of 2.2 and 4.0 ns for xPRO-SBA-**I** and xPRO-SBA-**I**′, respectively (see Section S7 for more details).

2.3.4. Potential Competitors

Having established the favorable detection features, we next assessed the response toward potentially competing metal ions. In a first experiment, the response of xPRO-SBA-**I** (0.11 mg mL^{-1}) toward excess amounts of the metal ions Mn^{II}, Co^{II}, Zn^{II}, Cd^{II}, Mg^{II}, Fe^{II}, Cu^{II}, Ni^{II}, Hg^{II}, and Ag^{I} was investigated. Figure 7 reveals that qualitatively the response pattern is not much different from that of **I** in aqueous solution. However, in line with a more hydrophobic environment around the probes adsorbed to the inner pore walls, $DF_{Hg/Ag}=4.4$ lies in between a value of 50 in water and 1.2 in MeCN (see above). Basically, the favorable selectivity of the probe is, thus, retained in xPRO-SBA-**I**. Therefore, the simple mix-&-load incorporation of a considerably small amount of **I** into a suitably modified mesoporous material allowed us to devise a hybrid material for trace Hg^{II} detection with excellent sensitivity and acceptable selectivity. In fact, the corresponding material that carries propyl groups on the inner and outer surfaces, PRO-SBA-**I**, showed sensitivity that was comparable to that of xPRO-SBA-**I** yet the selectivity was worse, that is, very similar to that of **I**, in MeCN. Neat SBA-**I** on the other hand was one order of magnitude less sensitive (see Section S4). Conclusively, suitable modification of the surface of mesoporous materials plays a key role in improving the selectivity and sensitivity.

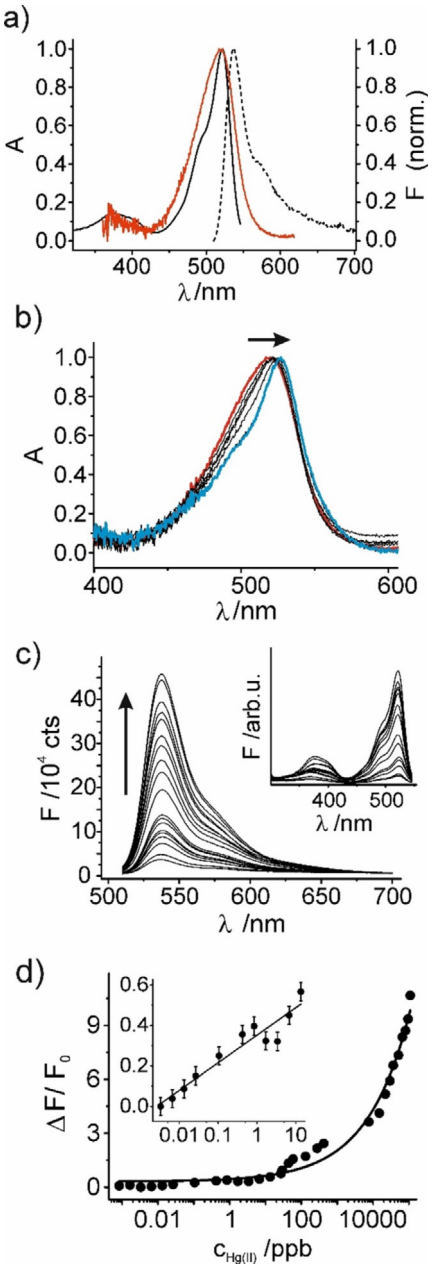

Figure 6. a) Absorption spectrum (red) and fluorescence excitation (solid black; $\lambda_{em}=564$ nm) and emission (dashed black; $\lambda_{ex}=490$ nm) spectra of xPRO-SBA-**I**′ in Milli-Q water (0.11 mg mL^{-1}; pH 7). b) Normalized absorption spectra of a suspension of xPRO-SBA-**I**′ in the presence of various amounts of Hg^{II}, increasing from red to blue. c) Fluorescence titration spectra ($\lambda_{ex}=490$ nm) of xPRO-SBA-**I**′ suspended in Milli-Q water (0.11 mg mL^{-1}; pH 7) upon the addition of Hg^{II}. Inset: Corresponding fluorescence excitation spectra ($\lambda_{em}=564$ nm). d) Corresponding fluorescence enhancement ratio ($\Delta F/F_0$) registered at $\lambda=538$ nm ($\lambda_{ex}=490$ nm) for xPRO-SBA-**I**′ suspended in Milli-Q water (0.11 mg mL^{-1}; pH 7) in the presence of increasing amounts of Hg^{II}. Inset: Magnification of the low-concentration range.

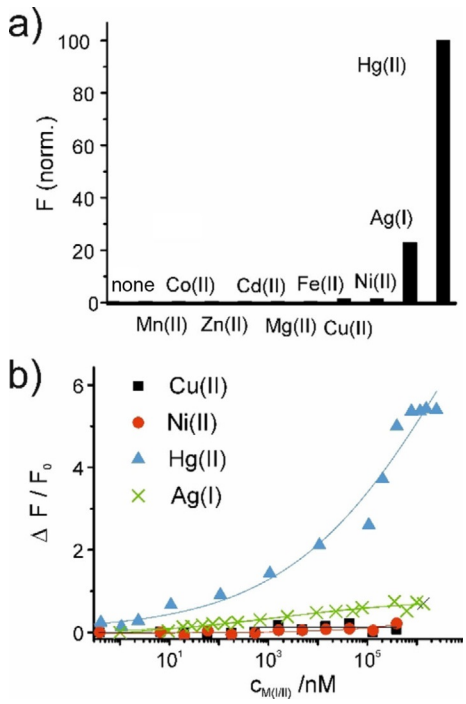

Figure 7. a) Intensity of fluorescence registered at $\lambda = 538$ nm ($\lambda_{ex} = 490$ nm) of xPRO-SBA-**I** suspended in Milli-Q water (0.11 mg mL^{-1}; pH 7) in the presence of 6 μM of Mn^{II}, Co^{II}, Zn^{II}, Cd^{II}, Mg^{II}, Fe^{II}, Cu^{II}, Ni^{II}, Hg^{II}, and Ag^{I}. b) Fluorescence enhancement in the corresponding suspensions as a function of the concentration of Ag^{I}, Hg^{II}, Ni^{II}, and Cu^{II}.

2.4. Mechanism at the Molecular Scale

So far, our tentative view of the analytical reaction is the complexation of Hg^{II} by the probe's crown ether receptor, and the probe is held by adsorptive forces at the pore wall. However, on the one hand, binding of the cation makes the **I**–Hg^{II} complex more polar than **I**, which can potentially lead to desorption of **I**–Hg^{II} into the solvent that fills the pores and, eventually, to release of the complex from the pores. On the other hand, although unmodified mesoporous silica materials are not exceptionally good binders for metal ions,[68] such as Hg^{II}, interaction of Hg^{II} with the inner pores' unmodified silanol groups can potentially displace probe molecules. To exclude the latter, we investigated xPRO-SBA-**II** as a control material that contains dye **II** and that has no metal-ion binding site (Scheme 1). Titration of xPRO-SBA-**II** with Hg^{II} did not lead to any fluorescence enhancement (Figure S7), excluding probe displacement as the active process. With respect to possible leaching of **I**–Hg^{II}, we incubated suspensions of the xPRO-SBA-**I**, xPRO-SBA-**II**, xPRO-SBA-**I**′, and PRO-N-**I**′ materials (0.11 mg mL^{-1}; pH 7) with various amounts of Hg^{II} for 30 min, centrifuged the samples, and measured the fluorescence of the remaining solution. Whereas no fluorescence was measured for the supernatants of SBA-type materials after centrifugation (even with high concentrations of Hg^{II}), strong fluorescence was observed in the supernatant of APT-N-**I**′, which indicates that in the absence of mesoporosity if **I** is only adsorbed to the outer surface of bulk silica the complex can easily desorb and transit to the solution. For PRO-N-**I**′, fluorescence in the absence of Hg^{II} was already strong, and the metal ion did not induce any sizeable enhancement (Figure S5). In addition, upon analyzing the residual solid materials after centrifugation under excitation with a $\lambda = 470$ nm LED and appropriate filters ($\lambda = 532$ nm cut-off filter, $\lambda = 550$ nm long-pass filter) in a homemade holder, fluorescence could only be detected for xPRO-SBA-**I**′ (Figure S8); no fluorescence was observed for APT-N-**I**′ (the fluorophore contents of xPRO-SBA-**I** and xPRO-SBA-**II** were too low to observe any fluorescence of the solid material under LED illumination). On the basis of these experiments, we can conclude that upon the addition of Hg^{II}, BODIPY probe **I** is released in the form of its complex from the surface of nonporous materials such as N-PRO-**I**′ yet it remains inside the pores for SBA-type mesoporous materials. These hybrid materials can thus not only detect but also scavenge the toxic metal ion.[69]

2.5. Determination of Hg^{II} in Natural Waters and Fish Tissues

Encouraged by the low LODs and the good discrimination against other environmentally relevant metal ions, we assessed the capability of xPRO-SBA-**I** for trace Hg^{II} determination in natural waters. Samples were collected from tap (Thailand), rivers (Germany and Vietnam), the Mediterranean Sea (Turkey) and lakes (Germany) possessing pH values between 6.3 and 6.7. An aliquot (2.5 mL) of each sample was mixed with a suspension (70 μL) of 4 mg mL^{-1} of xPRO-SBA-**I**, which led to a final concentration of 0.11 mg mL^{-1}, as also used in the previous optimization experiments. The Hg^{II} concentration in the waters was then determined by using the standard addition method and linear regression. For validation, the amount of Hg^{II} was also determined by cold vapor atomic fluorescence spectrometry (CV-AFS). As can be seen in Table 2, trace amounts of Hg^{II} were found in all cases, the values lying between 1 and 8 ppt, which are in agreement with contents found in uncontaminated waters by other authors.[70,71] In addition to the measurement of these background concentrations, we also spiked some of the samples with Hg^{II} and the recovery rates were excellent (Table 2).

To validate further the performance of the hybrid particle probe in complex sample matrices, a certified material of fish muscle ERM-BB422 with a known content of 0.601 ±

Table 2. Analysis of Hg^{II} in natural and spiked waters. Control experiments with natural water were also performed.

Sample	Hg^{II} spiked [ppt]	Hg^{II} found [ppt]	
		CV-AFS	xPRO-SBA-**I**
Müggelsee lake (DEU)	0	1.07 ± 0.08	1.4 ± 0.5
Müritz lake (DEU)	0	1.34 ± 0.06	1.0 ± 0.6
Spree river (DEU)	0	7.18 ± 2.70	9.9 ± 3.7
Teltow river (DEU)	0	1.45 ± 0.28	1.5 ± 0.7
Teltow river (DEU)	20.1	21.62 ± 0.43	21.5 ± 3.9
Baltic sea (DEU)	0	1.38 ± 0.38	0.8 ± 0.4
Mediterranean Sea (TUR)	0	0.97 ± 0.48	1.3 ± 0.6
tap water, Ko Samet (THA)	0	1.32 ± 0.20	1.1 ± 0.4
Da Nang river (VNM)	0	3.17 ± 0.70	2.8 ± 0.8
Nghe An river (VNM)	0	1.11 ± 0.47	1.0 ± 0.4
Nghe An river (VNM)	5	6.35 ± 0.77	5.9 ± 1.2

0.030 mg kg^{-1} CH_3Hg^+ (expressed as dry mass) was used. Contents of water in the certified material were estimated by depositing three samples of 1 g on Petri dishes and drying them overnight at 100 °C to yield a water content of 1.73 ± 0.18 %. Extraction of total mercury was performed by following reported procedures[72] using 1) ultrasound-assisted extraction procedure (UEP), 2) microwave-based acidic digestion method (MW), and 3) UV irradiation (see Section S6). All samples were analyzed with xPRO-SBA-**I** and by CV-AFS for validation in the way mentioned above, that is, by standard addition and linear regression. The results are summarized in Table 3 and show that the concentrations found by both methods for the extracts were in very good agreement. It was noted, however, that the extraction efficiency by the UEP method was comparatively low (≈25 %) and that the best efficiency was achieved with microwave digestion and HNO_3.

Table 3. Values of total mercury found in fish tissue extracts by using several extraction procedures and xPRO-SBA-**I** as well as CV-AFS.

Sample	Hg^{II} found[a] [mg kg^{-1}]	
	CV-AFS	xPRO-SBA-**I**
UEP-1	0.138 ± 0.004	0.134 ± 0.057
UEP-2	0.152 ± 0.008	0.156 ± 0.036
MW-1	0.546 ± 0.014	0.573 ± 0.054
MW-2	0.611 ± 0.006	0.598 ± 0.048
UV-1	0.540 ± 0.005	0.593 ± 0.044
UV-2	0.551 ± 0.008	0.567 ± 0.039

[a] Expressed as dried mass.

In an additional step towards real application, we analyzed several tissues from fishes purchased in a local supermarket. Mercury was extracted from portions of tissues of tuna, pollock, herring, and mackerel under UV irradiation, as described before, and the determination of Hg^{II} was performed in a way analogous to that used for the certified reference material. The results for xPRO-SBA-**I** summarized in Table 4 are again in accordance with those found by CV-AFS. They also comply well with values of mercury reported by the Food and Drug Administration Agency (FDA) on commercial fish and shellfish after a long-term study between 1990 and 2010.[73]

Table 4. Values of total mercury found in fish tissue extracts by using xPRO-SBA-**I** and CV-AFS.

Sample	Hg^{II} found[a] [mg kg^{-1}]		FDA value [mg kg^{-1}][41]
	CV-AFS	xPRO-SBA-**I**	
pollock	0.063 ± 0.004	0.058 ± 0.025	0.031 ± 0.086
tuna	0.442 ± 0.005	0.433 ± 0.082	0.391 ± 0.266
herring	0.127 ± 0.008	0.121 ± 0.013	0.084 ± 0.266
mackerel	0.052 ± 0.007	0.055 ± 0.024	0.05

[a] Expressed as dried mass.

2.6. Test Strips for Hg^{II} Determination

Although the performance of the particle probes in combination with 10 mm cells and a fluorometer offers a convenient alternative to classical laboratory-based methods, the hybrids are expected to unfold their true potential if implemented with even simpler detection formats such as test strips and a reader or mobile camera for data recording. Test strips are small and portable, fabricated from inexpensive materials, and, if combined with a suitable sensor or probe material, allow for the preparation of robust, quick, potent, easy-to-handle, simple, and potentially mass-producible assays for Hg^{II} determination. We thus spotted small volumes of a suspension of xPRO-SBA-**I** onto cellulose paper strips and employed the strips for the determination of Hg^{II} directly in water samples. A signal readout was accomplished with a lateral-flow (LF) fluorescence reader, which measures the integral fluorescence at a given excitation wavelength and detection filter settings, of the spots containing xPRO-SBA-**I**. In addition, pictures of the strips were taken with a camera (either digital or from a mobile communication device), and the differences in the relative luminance of the photographs of the strips taken under proper excitation conditions were analyzed to yield the respective data (see the Experimental Section for more details).

The strips were prepared by patterning hydrophobic walls of wax into a normal strip of cellulose filter paper. On each strip, a train of 13 spots containing xPRO-SBA-**I** or xPRO-SBA-**I**′ was deposited. Tests were conducted by spotting 2 μL of water onto the first spot, serving as a blank, and by spotting a series of 2 μL volumes containing different concentrations of Hg^{II} onto the following 12 spots. After drying, the fluorescence of the spots was registered with the LF reader and a photo was shot under excitation with an LED (λ_{ex} = 470 nm) and appropriate filters (λ = 532 nm cut-off filter, λ = 550 nm long-pass filter) in a homemade holder. As depicted in Figure 8, the spots showed a strong fluorescence enhancement in the presence of trace amounts of mercury. Moreover, the responses found by integrating the area of fluorescence of every spot on the strip as measured by the LF reader and by taking the mean coordinate number of the histogram of the *Y* coordinate of the *XYZ* coordinates of the CIE 1931 color space of each spot, quantifying the relative luminance changes, agree well. Table 5 lists the LODs found for the two read-out methods and the strips. It is clear that the analysis of luminance changes offers performance comparable to that of the reader. By again evaluating the responses of xPRO-SBA-**I** or xPRO-SBA-**I**′ we could reconfirm our previous findings, that is, a higher fluorescence enhancement with xPRO-SBA-**I**′ strips yet better sensitivity with xPRO-SBA-**I** strips. The strips thus present an ideal, simple tool for the determination of trace amounts of Hg^{II} in as-drawn water samples, covering well the concentration range around the EPA limit of 2 ppb. Of course, strip design is flexible, that is, the particle probes can be arranged in a way that only dipping into a sample is necessary. Moreover, if suitable reference spots are included, as we showed in previous work,[74] quantitative measurements with these rapid tests are

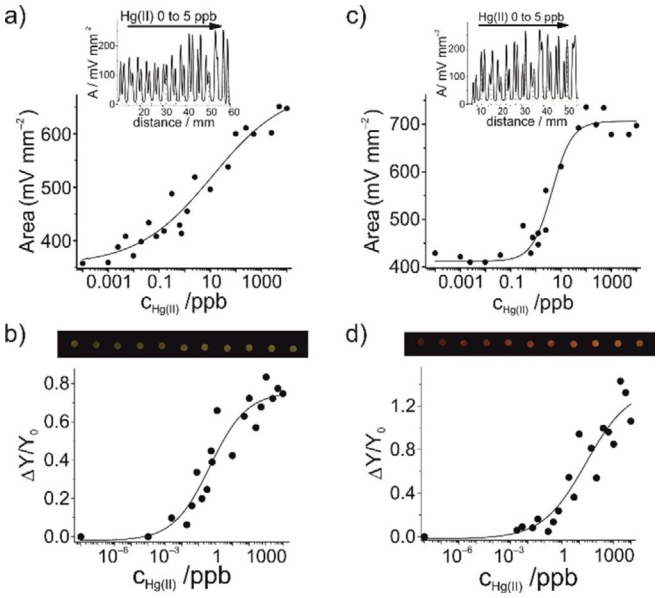

Figure 8. a, c) Areas of fluorescence ($\lambda_{ex}=470$ nm; $\lambda_{em}=520$ nm) on cellulose strips registered with a LF reader containing trains of spots of 2 μL suspension of a) xPRO-SBA-**I** (10 mg mL^{-1}) and c) xPRO-SBA-**I**′ (5 mg mL^{-1}) after the addition of 2 μL of solutions containing different amounts of Hg^{II}. Insets: Histograms of fluorescence. b, d) Relative changes in luminance (*Y* value of the CIE 1931 *XYZ* color space) for b) xPRO-SBA-**I** and d) xPRO-SBA-**I**′ strips as a function of Hg^{II} concentration. Insets: Photographs of the corresponding strips under irradiation with a homemade light source ($\lambda_{ex}=470$ nm). Hg^{II} concentrations from left to right: 0, 0. 02, 0.04, 0.08, 0.16, 0.32, 0.63, 1.25, 2.5, 5, and 10 ppb.

Table 5. LODs of Hg^{II} found from analysis of fluorescence intensities obtained with the reader and *Y* coordinate of *XYZ* CIE 1931 color space of photographs taken under a homemade excitation source ($\lambda_{ex}=470$ nm).

Sample	LOD [ppt] xPRO-SBA-**I**	xPRO-SBA-**I**′
reader	57	475
Y (luminance)	81	2900

straightforward, even if used outside of the laboratory by non-skilled personnel.

3. Conclusions

In this work, we reported the synthesis, characterization, and application of mesoporous materials that incorporate boron–dipyrromethene (BODIPY) probes by a simple mix-&-load technique and that allow for the sensitive and selective detection of Hg^{II} in aqueous samples by fluorescence enhancement in a simple mix-&-read format. Design followed the combination of a potent fluorescent probe, BODIPY **I**, that was sufficiently hydrophobic to adsorb at the inner pore walls of mesoporous silica with suitable chemical functionalization of the material's surface and choice of the optimum pore size. The best-performing hybrid, xPRO-SBA-**I**, retained the sterically embedded probe virtually quantitatively while avoiding dye aggregation and allowing the aqueous sample solution to diffuse rapidly into the pores and transport the analyte to the probes. Detailed mechanistic and analytical assessment revealed that the material performed well in terms of sensitive and selective determination of Hg^{II}, whether in suspension with a conventional fluorometer or on strip with a lateral-flow reader or a simple camera for signal recording. Determination of trace amounts of Hg^{II} in natural waters and in fish tissue extracts was performed and showed excellent agreement with cold-vapor atomic emission spectrometry (CV-AES) as a reference method. Finally, the simple mix-&-read test-strip assay demonstrated that this approach is very appealing for powerful and reliable analytics for everyday life in a relevant concentration range. If one considers that over the past four decades a vast number of small-molecule probes for a large number of analytes have been reported in the literature,[75–80] of which, however, only a few operate in neat aqueous solution, reconsideration of one or the other probe molecules and combination with suitably tailored nanomaterials in view of our present work might lead in a rather straightforward manner to various other potent indicator materials for comparatively simple analytical applications.

Experimental Section

Reagents and General Techniques

Chemicals and solvents were purchased from Sigma–Aldrich, Merck, and J.T. Baker in the highest quality available. Phosphate buffer and acetate buffer solutions (10 mM) were prepared with ultrapure reagent water, which was obtained by running demineralized water (by ion exchange) through a Milli-Q ultrapure water purification system (Millipore Synthesis A10). Absorption and fluorescence spectroscopy, elemental analysis, transmission electron microscopy (TEM), N_2 adsorption–desorption, dynamic light scattering (DLS), mass spectrometry, and NMR spectroscopy techniques were employed to characterize the synthesized materials and to test their behavior towards mercury and other cations. UV/Vis spectra were measured with a Specord 210plus from Analytik Jena. Fluorescence measurements were performed with a Fluoromax4 from HORIBA Scientific. Fluorescence lifetimes were determined with a unique customized laser impulse fluorometer with picosecond time resolution described elsewhere.[74,81] The fluorescence lifetime profiles were analyzed with a PC by using the software package FLA900 (Edinburgh Instruments). For all the spectroscopic experiments in water, a small amount of dye stock solution in MeCN was added to guarantee addition of a defined dye concentration. The final amount of MeCN was always $<0.2\,\%$ and had no influence on the spectroscopic results. Elemental analyses were determined by using a Euro EA-Elementaranalysator. TEM images were obtained with a Tecnai G2 20 Twin Transmission Electron Microscope, FEI Company, Oregon. N_2 adsorption–desorption isotherms were recorded with a Micromeritics ASAP2010 automated sorption analyzer. The samples were degassed at 200 °C in vacuum for 3 h. The specific surface areas were calculated from the adsorption data in the low-pressure range by using the BET model. Pore sizes were determined following the BJH method. DLS studies were conducted by using a Malvern Zetasizer Nano ZS. Mass spectra were measured with a CT Premier XE-TOF mass spectrometer. ^{1}H NMR and ^{13}C NMR spectra were acquired with Bruker AV-500 and AV-600 spectrometers by using residual protonated solvents as internal standards (^{1}H: $\delta[CDCl_3]=7.24$ ppm and ^{13}C: $\delta[CDCl_3]=77.23$ ppm).

Extraction of mercury from fish tissues was performed by using a UV lamp from LAR Analytik & Umweltmeßtechnik (NI. UO25E5; Tp: PLyser; 1991 V 230 KW 0'7), an ultrasonic bath from Elma-Hans Schmidbauer (Elmasonic P60), and a microwave from Anton Paar (Multi wave 3000). Control measurements of mercury were performed by cold vapor atomic emission spectroscopy (CV-AES) atomic fluorescence spectrometry (AFS) indicated in Section 2.5 using the mercury analyzer Mercur (Analytik Jena) and $SnCl_2$ as a reducing agent, following standard addition methods. A flow injection analysis system coupled to an atomic fluorescence spectrometer (FIAS-AF) from PerkinElmer was used for determination of Hg^{II} in the retention studies. A certified mercury solution of CertiPur quality (Merck) was used for producing the calibration samples. Before each series of measurements, a multipoint calibration was executed. Fluorescence measurements on strips were recorded with an ESE-Quant FL and a universal strip holder from Qiagen. Photographs were taken with a conventional digital camera (Canon PowerShot S90), and values of the RGB coordinates were obtained with the software ImageJ. The *Y* coordinate was calculated as a contribution of RGB coordinates according to 0.2126R + 0.7152G + 0.0722B by using Observer = 2° and Iluminant = DG5.[82]

Syntheses

BODIPY **I**: BODIPY **I** was prepared following a procedure adopted from our earlier works.[41,45,62] *p*-Formyl-*N*-phenyl-tetrathia-monoaza-15-crown-5 [4-(*N*-$AT_4$15C5)benzaldehyde; 146.0 mg, 0.379 mmol, 1 equiv.][62] and 4-ethyl-3,5-dimethylpyrrole (103.0 mg, 0.834 mmol, 2.2 equiv.) were dissolved in dry CH_2Cl_2 (70 mL) under an argon atmosphere. A few drops of trifluoroacetic acid were added, and the solution was stirred at room temperature in the dark until total consumption of the aldehyde (monitored by TLC). 2,3-Dichloro-5,6-dicyano-*p*-benzoquinone (DDQ; 90.8 mg, 0.4 mmol, 1.0 equiv.) was added, and the mixture was stirred for an additional 5 min. The mixture was then treated with *N*,*N*-diisopropylethylamine (500 μL, 2.8 mmol, 7.0 equiv.) and $BF_3{\cdot}OEt_2$ (550 μL, 4.4 mmol, 11.0 equiv.). After stirring for another 15 min, the dark solution was washed with water (3 × 50 mL). After extraction of the aqueous phase with CH_2Cl_2 (3 × 50 mL), the combined organic solution was dried (Na_2SO_4) and concentrated under reduced pressure. The crude product was purified by silica-gel flash column chromatography to yield shiny, orange crystals (70 mg, 29%). ^{1}H NMR (400 MHz, $CDCl_3$): δ = 0.99 (t, *J* = 7.6 Hz, 6H, 2CH_2-CH_3), 1.36 (s, 6H, 2C-CH_3), 2.30 (q, *J* = 7.5 Hz, 4H, 2CH_2-CH_3), 2.52 (s, 6H, 2*N*-C-CH_3), 2.86 (m, 16H, 4CH_2-S-CH_2), 3.67 (m, 4H, 2*N*-CH_2), 6.91 (d, *J* = 8.7 Hz, 4H, 4CH_{ar}), 7.14 ppm (d, *J* = 8.8 Hz, 4H, 4CH_{ar}). HRMS (ESI+): *m*/*z*: calcd for $C_{33}H_{47}BF_2N_3S_4$: 662.2714 $[M+H]^+$; found: 662.2721.

BODIPY **II**: BODIPY **II** was synthesized as reported previously by us.[45]

Mesoporous SBA-15 silica microparticles (SBA): SBA-15 was synthesized as reported previously[83] with triblock poly(ethylene oxide)–poly(propylene oxide)–poly(ethylene oxide) (EO_{20}-PO_{70}-EO_{20}, P123) copolymer as a structure-directing agent and tetraethylorthosilicate (TEOS) as a silica source. In a typical synthesis, P123 (4.0 g, 0.69 mmol) was dissolved in water (120 mL) and HCl (19.41 mL), and the mixture was stirred at 35 °C for 1 h to dissolve the polymer. Then, TEOS (9.15 mL, 41 mmol) was added dropwise into the homogeneous solution with stirring at 35 °C for 24 h. The obtained gel was aged at 100 °C in a Teflon flask without stirring for 48 h. The white solid obtained was filtered, washed with distilled water, and air dried at 70 °C in a vacuum for 12 h.

xPRO-SBA: For a nonuniform distribution of propyl groups on the material's surface, 250 mg of as-synthesized SBA-15 was suspended in a flask containing MeCN (7.5 mL) before propyltrimethoxysilane (220.2 μL, 5 mmol g_{solid}^{-1}) was added to the suspension to anchor the propyl chains preferentially on the outer surface of SBA-15. The suspension was stirred at room temperature for 5.5 h, and afterwards, the solid was centrifuged for 5 min at 10.000 rpm, washed with MeCN (2 × 5 mL), and dried in a vacuum. In a second step, the organic template of the silica material expressing propyl groups was removed by extraction with HCl in EtOH. For this purpose, the solid (250 mg) previously prepared was suspended in a mixture of HCl (0.1 mL) and EtOH (25 mL), and the suspension was stirred at 100 °C for 15 h. After that, the solid was centrifuged for 5 min at 10.000 rpm, washed with water until neutral pH, and dried in a vacuum.

xPRO-SBA-**I**: A solution of **I** was prepared in MeCN at a concentration of 26 μmol L^{-1}. Next, xPRO-SBA (20 mg) was suspended in a solution of BODIPY **I** (4 mL, final concentration of **I** = 5 μmol$_{\mathbf{I}}$ g_{solid}^{-1}), and the suspension was stirred at room temperature for 24 h. The suspension was then centrifuged (10 min at 6000 rpm) and was washed several times with water until no fluorescence was observed in the supernatants under the UV lamp. Finally, the solid was dried in a vacuum for 12 h.

xPRO-SBA-**I**′: Solid xPRO-SBA-**I**′ was prepared following the same procedure as that outlined for xPRO-SBA-**I** except for the use of an initial solution of **I** of 1.05 mmol L^{-1} (arriving at suspensions with a final concentration of 200 μmol$_{\mathbf{I}}$ g_{solid}^{-1}).

xPRO-SBA-**II**: Solid xPRO-SBA-**II** was prepared following the same procedure as that outlined for xPRO-SBA-**I** only replacing a solution of BODIPY **I** for the corresponding BODIPY **II**. xPRO-SBA (20 mg) was suspended in BODIPY **II** solution (4 mL, 26 μmol L^{-1}) in MeCN to obtain a suspension with a final concentration of 5 μmol$_{\mathbf{II}}$ g_{solid}^{-1}. After 24 h of agitation at room temperature, the material was washed several times with water and dried in a vacuum.

Test strips: The strips were prepared by patterning hydrophobic walls of wax into a normal cellulose filter paper (Whatman No. 1) by using a commercially available printer (Xerox ColorQube 8580 AND), followed by baking in an oven at 110 °C for 2 min to melt the wax and to create the hydrophobic barriers across the entire thickness of the paper. Strips of 0.5 × 5 cm containing 13 sensing spots of 3 mm diameter were designed for the experiments. Several strips were prepared, spotting suspensions (2 μL) of xPRO-SBA-**I** (10 mg mL^{-1}) or xPRO-SBA-**I**′ (5 mg mL^{-1}) in water for each spot. Strips were left at room temperature to dry.

Acknowledgements

Financial support from the Alexander von Humboldt Foundation and Germany's Federal Ministry for Economic Affairs and Energy is gratefully acknowledged. We thank Sören Selve (Technical University Berlin) for TEM images, Andrea Zehl (Humboldt University Berlin) for elemental analysis, Dietmar Pfeifer and Christian Jäger (BAM, Div. 1.3) for NMR spectroscopy support, Annett Zimathies (BAM, Div. 1.3) for N_2 adsorption–desorption measurements, Sibylle Penk (BAM, Div. 1.6) for the microwave extraction of Hg^{II}, Raúl Gotor (BAM, Div. 1.9) for the assembly of the homemade fluorescence lamp, Tobias Fischer (BAM, Div. 1.9) for support with the fluorescence decay measurements, and Karina Fast (BAM, Div. Z.8) for the cover graphics.

Conflict of Interest

The authors declare no conflict of interest.

Keywords: dyes/pigments · fluorescence · mercury · mesoporous materials · test strips

[1] E. M. Nolan, S. J. Lippard, *J. Am. Chem. Soc.* **2007**, *129*, 5910 – 5918.
[2] B. Gworek, O. Bemowska-Kalabun, M. Kijenska, J. Wrzosek-Jakubowska, *Water Air Soil Pollut.* **2016**, *227*, 371.
[3] P. Holmes, K. A. F. James, L. S. Levy, *Sci. Total Environ.* **2009**, *408*, 171 – 182.
[4] K. Sundseth, J. M. Pacyna, E. G. Pacyna, N. Pirrone, R. J. Thorne, *Int. J. Environ. Res. Public Health* **2017**, *14*, 105.
[5] R. Ebinghaus, H. Hintelmann, R. D. Wilken, *Fresenius J. Anal. Chem.* **1994**, *350*, 21 – 29.
[6] H. Hsu-Kim, K. H. Kucharzyk, T. Zhang, M. A. Deshusses, *Environ. Sci. Technol.* **2013**, *47*, 2441 – 2456.
[7] S. M. Ullrich, T. W. Tanton, S. A. Abdrashitova, *Crit. Rev. Environ. Sci. Technol.* **2001**, *31*, 241 – 293.
[8] Commission Regulation (EC) No 1881/2006 of 19 December 2006 setting maximum levels for certain contaminants in foodstuff *Off. J. Eur. Union* **2006**, L364/5 – L364/24.
[9] J. Barton, M. B. G. García, D. H. Santos, P. Fanjul-Bolado, A. Ribotti, M. McCaul, D. Diamond, P. Magni, *Microchim. Acta* **2016**, *183*, 503 – 517.
[10] K. Duarte, C. I. L. Justino, A. C. Freitas, A. M. P. Gomes, A. C. Duarte, T. A. P. Rocha-Santos, *TrAC Trends Anal. Chem.* **2015**, *64*, 183 – 190.
[11] F. Zarlaida, M. Adlim, *Microchim. Acta* **2017**, *184*, 45 – 58.
[12] A. B. Descalzo, R. Martínez-Máñez, R. Radeglia, K. Rurack, J. Soto, *J. Am. Chem. Soc.* **2003**, *125*, 3418 – 3419.
[13] H. H. Harris, I. J. Pickering, G. N. George, *Science* **2003**, *301*, 1203 – 1203.
[14] J. V. Ros-Lis, M. D. Marcos, R. Mártinez-Máñez, K. Rurack, J. Soto, *Angew. Chem. Int. Ed.* **2005**, *44*, 4405 – 4407; *Angew. Chem.* **2005**, *117*, 4479 – 4482.
[15] S. V. Wegner, A. Okesli, P. Chen, C. He, *J. Am. Chem. Soc.* **2007**, *129*, 3474 – 3475.
[16] J. Bell, E. Climent, M. Hecht, M. Buurman, K. Rurack, *ACS Sens.* **2016**, *1*, 334 – 338.
[17] Y. Ding, S. Wang, J. Li, L. Chen, *TrAC Trends Anal. Chem.* **2016**, *82*, 175 – 190.
[18] J. Du, L. Jiang, Q. Shao, X. Liu, R. S. Marks, J. Ma, X. Chen, *Small* **2013**, *9*, 1467 – 1481.
[19] Z. Sun, J. Du, C. Jing, *J. Environ. Sci.* **2016**, *39*, 134 – 143.
[20] L. R. Pokhrel, N. Ettore, Z. L. Jacobs, A. Zarr, M. H. Weir, P. R. Scheuerman, S. R. Kanel, B. Dubey, *Sci. Total Environ.* **2017**, *574*, 1379 – 1388.
[21] X. Xu, Y.-F. Li, J. Zhao, Y. Li, J. Lin, B. Li, Y. Gao, C. Chen, *Analyst* **2015**, *140*, 7841 – 7853.
[22] G. Chen, Z. Guo, G. Zeng, L. Tang, *Analyst* **2015**, *140*, 5400 – 5443.
[23] H. N. Kim, W. X. Ren, J. S. Kim, J. Yoon, *Chem. Soc. Rev.* **2012**, *41*, 3210 – 3244.
[24] P. Mahato, S. Saha, P. Das, H. Agarwalla, A. Das, *RSC Adv.* **2014**, *4*, 36140 – 36174.
[25] M. B. Gumpu, S. Sethuraman, U. M. Krishnan, J. B. B. Rayappan, *Sens. Actuators B* **2015**, *213*, 515 – 533.
[26] J. Liu, Y. Lu, *Angew. Chem. Int. Ed.* **2007**, *46*, 7587 – 7590; *Angew. Chem.* **2007**, *119*, 7731 – 7734.
[27] C.-K. Chiang, C.-C. Huang, C.-W. Liu, H.-T. Chang, *Anal. Chem.* **2008**, *80*, 3716 – 3721.
[28] D. Li, A. Wieckowska, I. Willner, *Angew. Chem. Int. Ed.* **2008**, *47*, 3927 – 3931; *Angew. Chem.* **2008**, *120*, 3991 – 3995.
[29] J. Wang, B. Liu, *Chem. Commun.* **2008**, 4759 – 4761.
[30] B.-C. Ye, B.-C. Yin, *Angew. Chem. Int. Ed.* **2008**, *47*, 8386 – 8389; *Angew. Chem.* **2008**, *120*, 8514 – 8517.
[31] R. Freeman, T. Finder, I. Willner, *Angew. Chem. Int. Ed.* **2009**, *48*, 7818 – 7821; *Angew. Chem.* **2009**, *121*, 7958 – 7961.
[32] S. Botasini, G. Heijo, E. Méndez, *Anal. Chim. Acta* **2013**, *800*, 1 – 11.
[33] E. Chung, R. Gao, J. Ko, N. Choi, D. W. Lim, E. K. Lee, S.-I. Chang, J. Choo, *Lab Chip* **2013**, *13*, 260 – 266.
[34] S. Gómez-de Pedro, D. Lopes, S. Miltsov, D. Izquierdo, J. Alonso-Chamarro, M. Puyol, *Sens. Actuators B* **2014**, *194*, 19 – 26.
[35] W. Chen, X. Fang, H. Li, H. Cao, J. Kong, *Sci. Rep.* **2016**, *6*, 31948.
[36] F. Liu, S. Wang, M. Zhang, Y. Wang, S. Ge, J. Yu, M. Yan, *Microchim. Acta* **2014**, *181*, 663 – 670.
[37] Y. Zhang, P. Zuo, B.-C. Ye, *Biosens. Bioelectron.* **2015**, *68*, 14 – 19.
[38] J. W. Grate, G. C. Frye, *Sensors Update*, Wiley-VCH, Weinheim, **1996**.
[39] J. Ishikawa, H. Sakamoto, H. Wada, *J. Chem. Soc. Perkin Trans. 2* **1999**, 1273 – 1280.
[40] K. Rurack, J. L. Bricks, J. L. Slominski, U. Resch-Genger in *Near-Infrared Dyes for High Technology Applications* (Eds.: S. Dähne, U. Resch-Genger, O. S. Wolfbeis), Kluwer Academic, Dordrecht, **1998**, pp. 191 – 200.
[41] K. Rurack, M. Kollmannsberger, U. Resch-Genger, J. Daub, *J. Am. Chem. Soc.* **2000**, *122*, 968 – 969.
[42] A. Loudet, K. Burgess, *Chem. Rev.* **2007**, *107*, 4891 – 4932.
[43] M. Shah, K. Thangaraj, M.-L. Soong, L. T. Wolford, J. H. Boyer, I. R. Politzer, T. G. Pavlopoulos, *Heteroat. Chem.* **1990**, *1*, 389 – 399.
[44] F. Bergström, I. Mikhalyov, P. Hägglöf, R. Wortmann, T. Ny, L. B. Å. Johansson, *J. Am. Chem. Soc.* **2002**, *124*, 196 – 204.
[45] M. Hecht, W. Kraus, K. Rurack, *Analyst* **2013**, *138*, 325 – 332.
[46] E. Climent, M. Biyikal, K. Gawlitza, T. Dropa, M. Urban, A. M. Costero, R. Martínez-Máñez, K. Rurack, *Sens. Actuators B* **2017**, *246*, 1056 – 1065.
[47] J. Opel, M. Hecht, K. Rurack, J. Eiblmeier, W. Kunz, H. Colfen, M. Kellermeier, *Nanoscale* **2015**, *7*, 17434 – 17440.
[48] S. Zhu, J. Zhang, G. Vegesna, F.-T. Luo, S. A. Green, H. Liu, *Org. Lett.* **2011**, *13*, 438 – 441.
[49] T. Komatsu, D. Oushiki, A. Takeda, M. Miyamura, T. Ueno, T. Terai, K. Hanaoka, Y. Urano, T. Mineno, T. Nagano, *Chem. Commun.* **2011**, *47*, 10055 – 10057.
[50] L. Li, J. Han, B. Nguyen, K. Burgess, *J. Org. Chem.* **2008**, *73*, 1963 – 1970.
[51] S.-l. Niu, C. Massif, G. Ulrich, P.-Y. Renard, A. Romieu, R. Ziessel, *Chem. Eur. J.* **2012**, *18*, 7229 – 7242.
[52] X. S. Zhao, G. Q. Lu, A. K. Whittaker, G. J. Millar, H. Y. Zhu, *J. Phys. Chem. B* **1997**, *101*, 6525 – 6531.
[53] A. B. Descalzo, M. Dolores Marcos, C. Monte, R. Martinez-Manez, K. Rurack, *J. Mater. Chem.* **2007**, *17*, 4716 – 4723.
[54] X. S. Zhao, G. Q. Lu, X. Hu, *Microporous Mesoporous Mater.* **2000**, *41*, 37 – 47.
[55] M. W. Hornung, P. M. Cook, K. M. Flynn, D. B. Lothenbach, R. D. Johnson, J. W. Nichols, *Aquat. Toxicol.* **2004**, *67*, 1 – 11.
[56] A. B. Descalzo, K. Rurack, H. Weisshoff, R. Martínez-Máñez, M. D. Marcos, P. Amorós, K. Hoffmann, J. Soto, *J. Am. Chem. Soc.* **2005**, *127*, 184 – 200.
[57] A. B. Descalzo, R. Martinez-Manez, R. Sancenon, K. Hoffmann, K. Rurack, *Angew. Chem. Int. Ed.* **2006**, *45*, 5924 – 5948; *Angew. Chem.* **2006**, *118*, 6068 – 6093.
[58] R. Gotor, P. Ashokkumar, M. Hech, K. Keil, K. Rurack, *Anal. Chem.* **2017**, *89*, 8437 – 8444.
[59] M. Kollmannsberger, K. Rurack, U. Resch-Genger, J. Daub, *J. Phys. Chem. A* **1998**, *102*, 10211 – 10220.
[60] J.-P. Malval, I. Leray, B. Valeur, *New J. Chem.* **2005**, *29*, 1089 – 1094.
[61] H. W. Mbatia, D. P. Kennedy, C. E. Camire, C. D. Incarvito, S. C. Burdette, *Eur. J. Inorg. Chem.* **2010**, 5069 – 5078.
[62] K. Rurack, J. L. Bricks, G. Reck, R. Radeglia, U. Resch-Genger, *J. Phys. Chem. A* **2000**, *104*, 3087 – 3109.
[63] J. Du, J. Fan, X. Peng, H. Li, J. Wang, S. Sun, *J. Fluoresc.* **2008**, *18*, 919 – 924.
[64] J. Fan, K. Guo, X. Peng, J. Du, J. Wang, S. Sun, H. Li, *Sens. Actuators B* **2009**, *142*, 191 – 196.
[65] S. C. Dodani, Q. He, C. J. Chang, *J. Am. Chem. Soc.* **2009**, *131*, 18020 – 18021.
[66] M. Royzen, A. Durandin, V. G. Young, N. E. Geacintov, J. W. Canary, *J. Am. Chem. Soc.* **2006**, *128*, 3854 – 3855.
[67] F. L. Arbeloa, P. R. Ojeda, I. L. Arbeloa, *J. Chem. Soc. Faraday Trans. 2* **1988**, *84*, 1903 – 1912.
[68] L. Mercier, T. J. Pinnavaia, *Adv. Mater.* **1997**, *9*, 500 – 503.
[69] J. V. Ros-Lis, R. Casasus, M. Comes, C. Coll, M. D. Marcos, R. Martinez-Manez, F. Sancenon, J. Soto, P. Amoros, J. El Haskouri, N. Garro, K. Rurack, *Chem. Eur. J.* **2008**, *14*, 8267 – 8278.
[70] J. M. Benoit, C. C. Gilmour, R. P. Mason, G. S. Riedel, G. F. Riedel, *Biogeochemistry* **1998**, *40*, 249 – 265.

[71] F. J. G. Laurier, R. P. Mason, G. A. Gill, L. Whalin, *Mar. Chem.* **2004**, *90*, 3 – 19.
[72] A. Q. Shah, T. G. Kazi, J. A. Baig, H. I. Afridi, G. A. Kandhro, S. Khan, N. F. Kolachi, S. K. Wadhwa, *Pak. J. Anal. Environ. Chem.* **2010**, *11*, 12 – 17.
[73] Mercury Levels in Commercial Fish and Shellfish (1990 – 2012), FDA 1990 – 2012, https://www.fda.gov/food/foodborneillnesscontaminants/metals/ucm115644.htm.
[74] P. Ashokkumar, H. Weisshoff, W. Kraus, K. Rurack, *Angew. Chem. Int. Ed.* **2014**, *53*, 2225 – 2229; *Angew. Chem.* **2014**, *126*, 2257 – 2261.
[75] A. P. de Silva, H. Q. N. Gunaratne, T. Gunnlaugsson, A. J. M. Huxley, C. P. McCoy, J. T. Rademacher, T. E. Rice, *Chem. Rev.* **1997**, *97*, 1515 – 1566.
[76] R. Martínez-Máñez, F. Sancenon, *Chem. Rev.* **2003**, *103*, 4419 – 4476.
[77] J. Li, D. Yim, W. D. Jang, J. Yoon, *Chem. Soc. Rev.* **2017**, *46*, 2437 – 2458.
[78] S. A. Rommel, D. Sorsche, M. Fleischmann, S. Rau, *Chem. Eur. J.* **2017**, *23*, 18101 – 18119.
[79] T. Rasheed, M. Bilal, F. Nabeel, H. M. N. Iqbal, C. L. Li, Y. F. Zhou, *Sci. Total Environ.* **2018**, *615*, 476 – 485.
[80] A. B. Aletti, D. M. Gillen, T. Gunnlaugsson, *Coord. Chem. Rev.* **2018**, *354*, 98 – 120.
[81] Z. Shen, H. Röhr, K. Rurack, H. Uno, M. Spieles, B. Schulz, G. Reck, N. Ono, *Chem. Eur. J.* **2004**, *10*, 4853 – 4871.
[82] For more information, see http://www.easyrgb.com.
[83] E. Climent, M. Biyikal, K. Gawlitza, T. Dropa, M. Urban, A. M. Costero, R. Martínez-Máñez, K. Rurack, *Chem. Eur. J.* **2016**, *22*, 11138 – 11142.

Received: June 12, 2018

